Loughney, K.M., et al., 2023, **Middle Miocene fire activity and C_4 vegetation expansion in the Barstow Formation, California:** Geology, https://doi.org/10.1130/G50881.1

Supplemental Material

Methods and Figure S1.

Supplemental Table S1

SUPPLEMENTAL MATERIAL

METHODS

Field methods

Sediment samples were collected over several field seasons (2014–2016) from 19 stratigraphic sections in the Mud Hills, California (Fig. 1), at approximately 20-meter intervals for paleoenvironmental indicators (Loughney et al., 2020). Sample lithologies were claystone, siltstone, and sandy siltstone. These samples span the thickness of the Barstow Formation and include all members and facies associations in the Mud Hills (Loughney and Badgley, 2017). Twenty-six samples were selected for this study based on phytoclast presence noted during analyses of phytoliths (Loughney and Smith, 2015; Loughney et al., 2020). The estimated ages of the samples range from 16.5 to 13.3 Ma. Age estimates are based on an absolute age model created using the Bchron package, version 4.7.1 (Haslett and Parnell, 2008), in R version 4.2.1 (R Core Team, 2020). The model was calibrated using radiometric ages on tuff horizons and carbonates from MacFadden et al. (1990), Woodburne et al. (1990), Cole et al. (2005), Miller et al. (2022), and Eden et al. (2023). All field work and sampling were done in accordance with permits issued to Badgley from the Bureau of Land Management.

Laboratory methods

Sediment samples were prepared for microscopic charcoal analysis in a process adapted from Rhodes (1998) and Schüpbach et al. (2015) for modern soil samples. This process was chosen for its simple material and resource requirements, compared to other methods for charcoal extraction from ancient samples that involve specialized equipment or hazardous materials (i.e., HF). Rhodes (1998) and Schüppach et al. (2015) used 0.2 g and 1.0 cm^3 of sample, respectively, in their analyses; due to the anticipated low presence of charred particles in

the Miocene samples, we processed 5 g of sediment for each sample. Samples were weighed, crushed, and covered with a deflocculating solution of 5% (0.082 mol/L) sodium hexametaphosphate ($(NaPO_3)_6$) in order to facilitate disaggregation. Samples were soaked in the deflocculating solution for four hours and then desiccated at 50°C for 24 hours. Samples were then treated with 20 mL of 6% (1.77 mol/L) hydrogen peroxide (H_2O_2) and dried at 50°C for 24 hours. This step aids charcoal identification by bleaching dark mineral grains while leaving the charred grains unaffected. Because no macroscopic grains were observed prior to and during processing, samples were washed through a 250-μm mesh sieve with deionized water in order to capture all potential grain sizes. The fine fraction was then washed into petri dishes with deionized water for counting.

Analytical methods

We counted the total number of microscopic charred grains visible at 50x magnification using a Nikon SMZ 1500 light microscope. Charcoal grains can be broadly divided into macroscopic (>125 μm), mesoscopic (125–50 μm), and microscopic (50–10 μm) size classes (Vachula, 2019). Samples were analyzed wet to aid with identification of charcoal grains based on characteristics including dark color, shape, and three-dimensionality (most charcoal grains are robustly three-dimensional, in contrast to planar mineral grains such as mica). Organic material is rare in the Barstow Formation, and we considered observed dark-colored phytoclasts to be charred particles rather than unburned plant material or coal (see below).

Charcoal-accumulation rate. The total grain count and volume of each sample and sedimentation rate of facies associations (Table S1) were used to determine the charcoal-accumulation rate (Table S2). Charcoal-accumulation rates (CHAR) approximate the number of

charcoal grains deposited each year on a square centimeter of sediment (grains cm^{-2} yr^{-1}; Higuera et al., 2010):

CHAR = number of charcoal grains per volume of sediment × sediment-accumulation rate. (1)

Sample volume (cm^3) was calculated using the mass of the weighed sample and the density of the sediment, which was estimated as 2.6 g/cm^3, based on the average density of mixed siliciclastic sediment (containing quartz, feldspars, and clays). We used the average sediment-accumulation rates (SAR) of each of the six facies associations (FA) in the Barstow Formation (in cm/yr; Table S1) to calculate the FA-specific CHAR of each sample. SARs were calculated using age estimates from MacFadden et al. (1990), Woodburne et al. (1990), Woodburne (1996), and Cole et al. (2005).

Confidence intervals. In charcoal analyses from Quaternary sediment records, a threshold CHAR value is used to distinguish peaks from background rates of accumulation through detrending and resampling (Higuera et al., 2010). Abundance peaks represent fire episodes which consist of one or more fires (Whitlock and Larsen, 2001). Because our analyses involve fewer samples spanning much larger time intervals than modern analyses, and our samples represent a variety of depositional environments, we could not generate a robust estimate of background levels of accumulation. We instead used confidence intervals generated from a bootstrapped resampling procedure of sample CHAR values (code provided below). The mean CHAR of all 26 samples for the formation was calculated with replacement 1000 times to generate upper and lower 95% confidence limits. Omitting one sample without charred particles slightly increased the upper and lower limits but did not significantly change the range of the confidence interval. We used a jackknife resampling procedure to generate 95% confidence

intervals for concentration and CHAR of samples from each FA (Table 1). We consider values outside the confidence interval as potentially indicative of increased fire activity, and outlier values >2σ above the formation mean as strongly indicative of increased fire activity. Calculations were performed in R version 4.2.1 (R Core Team, 2020) and using dplyr version 1.0.10 (Wickham et al., 2022).

RESULTS AND DISCUSSION

Charred particle identification

Twenty-five samples (96%) had charred particles (Table S3). All charred grains were <100 μm, with most grains measuring 5 to 10 μm in length. This range is less than the commonly accepted lower limit for microscopic charcoal (<10 μm; Vachula, 2019). Particles in this size range may be characterized more generally as black carbon, which encompasses ash, char, and charcoal (Scott, 2010). Black carbon particles are products of fire and are used as fire indicators, although there is a lack of consensus on definitions and terminology for very small particles (Schmidt and Noack, 2000). In addition, very small black carbon or charred particles may be difficult to distinguish from other black phytoclasts such as redeposited coal and plant material. Coal does not occur in the Barstow Formation, and this is unlikely to be a source of small phytoclasts. Horizons bearing carbonized root traces occur in the formation but were not sampled for charcoal analyses. We therefore consider the observed microscopic particles to be black carbon derived from burned plant material rather than other types of phytoclasts.

Fracturing of charred particles can occur during transport and deposition (Scott, 2010). It is probable that fracturing of charred grains occurred both diagenetically and during sample processing, affecting the perceived versus actual amount of microscopic black carbon, and

contributing to the small size fraction of the particles. All samples were processed with the same gentle crushing method. However, the large range of particle counts among samples (0–1159) indicates that differences in black carbon concentration are real and that processing methods did not significantly inflate the observed amount of black carbon.

Carbon isotopes

Carbon isotopic data from compound-specific biomarkers ($\delta^{13}C_{alk}$) and soil organic matter ($\delta^{13}C_{SOM}$) from the Barstow Formation show a general enrichment trend through time. Differences in carbon systems, however, cause the $\delta^{13}C_{alk}$ and $\delta^{13}C_{SOM}$ records to fluctuate and to respond to different climatic and environmental factors. The $\delta^{13}C_{alk}$ record is derived from *n*-alkanes of terrestrial plants and closely follows atmospheric pCO_2, which increased through the Miocene Climatic Optimum and decreased after ~15 Ma (Tipple et al., 2010). $\delta^{13}C$ from bulk soil organic matter potentially derives from numerous organic compounds and may incorporate the effects of soil decomposition processes during formation (Wynn, 2007). $\delta^{13}C_{alk}$ and $\delta^{13}C_{SOM}$ values may also show differing trends owing to differences in fractionation of carbon between original plant sources (see Loughney et al., 2020 and references therein).

Environmental and facies influences on black carbon preservation

The black carbon record from the Barstow Formation illustrates the complex relationship of changing climate and habitat and their effects on black carbon preservation. Many factors may affect black carbon preservation in ancient records, contributing to the variation in FA-specific CIs. Sediment-accumulation rates (SAR) vary among depositional environments, and in modern settings, local sedimentary processes can increase the accumulation of charcoal (Patterson et al., 1987; Whitlock and Millspaugh, 1996; Whitlock and Larson, 2001). Facies associations of the Barstow Formation represent alluvial-fan, lacustrine, channel, and floodplain environments with

differing SARs, which generally decreased through time with the changing dominant environments (Table S1; Loughney and Badgley, 2017). This trend contrasts with the trend in CHAR, in which the highest values occur in FAs with the lowest SARs (Table 1).

Variation in black carbon concentration and CHAR among FAs may also reflect differences in depositional environments and their potential to accumulate and preserve charred particles. Samples with the highest CHAR were from FA 6, which represents seasonally dry savanna (Loughney et al., 2020). The abundance of grains from this FA may relate to the ability of open-canopy environments to accumulate greater amounts of wind-blown charcoal than closed-canopy habitats (Aleman et al., 2013). FA 2 represents shallow lacustrine environments, which may similarly have contributed to the greater abundance of black carbon in these samples than in samples from FAs that represent more closed-canopy environments (Table 1). Differences in time averaging may also contribute to the variation in concentration and CHAR among samples, as lower SARs in ephemeral-wetland (FA 6) and ponded-floodplain (FA 5) settings would concentrate black carbon over longer periods of time than channel and proximal-floodplain settings (FA 1, 3, 4) with higher SARs (Loughney and Badgley, 2017). Once accumulated, black carbon in lower-energy settings would have been less likely to be reworked than in higher-energy settings. The low SAR and open-canopy habitats represented by FA 6 may have allowed charred particles to accumulate over longer periods of time, contributing to their abundance in the uppermost part of the formation.

References

Aleman, J.C., Blarquez, O., Bentaleb, I., Bonté, P., Brossier, B., Carcaillet, C., Gond, V., Gourlet-Fleury, S., Kpolita, A., Lefèvre, I., Oslisly, R., Power, M.J., Yongo, O., Bremond, L., Favier, C., 2013, Tracking land-cover changes with sedimentary charcoal in the Afrotropics: The Holocene, v. 23, no. 12, p. 1853–1862. Doi: 10.1177/0959683613508159.

Cole, J.M., Rasbury, E.T., Hanson, G.N., Montañez, I.P., and Pedone, V.A., 2005, Using U-Pb ages of Miocene tufa for correlation in a terrestrial succession, Barstow Formation, California: Geological Society of America Bulletin, v. 117, no. 3–4, p. 276–287.

Eden, R., Gans, P., and Cottle, J., 2023, Tephrachronology of the Miocene Barstow Formation, western Mojave, CA, *in* Miller, D.M., and Rowland, S.M., eds., Mines of the Mojave: The 2023 Desert Symposium Field Guide and Proceedings: Zzyzx, California, Desert Symposium, Inc., p. 167–168.

Haslett, J., and Parnell, A.C., 2008, A simple monotone process with application to radiocarbon-dated depth chronologies: Journal of the Royal Statistical Society: Series C (Applied Statistics), v. 57, no. 4, p. 399–418.

Higuera, P.E., Gavin, D.G., Bartlein, P.J., and Hallett, D.J., 2010, Peak detection in sediment–charcoal records: Impacts of alternative data analysis methods on fire-history interpretations: International Journal of Wildland Fire, v. 19, p. 996–1014.

Loughney, K.M., and Smith, S.Y., 2015, Phytoliths from the Barstow Formation through the Middle Miocene Climatic Optimum: Preliminary results, *in* Reynolds, R.E., ed., Mojave Miocene: The 2015 Desert Symposium Field Guide and Proceedings: Zzyzx, California, California State University Desert Studies Consortium, p. 51–58.

Loughney, K.M., and Badgley, C., 2017, Facies, environments, and fossil preservation in the Barstow Formation, Mojave Desert, California: PALAIOS, v. 32, no. 6, p. 396–412.

Loughney, K.M., Hren, M.T., Smith, S.Y., and Pappas, J.L., 2020, Vegetation and habitat change in southern California through the Middle Miocene Climatic Optimum: Paleoenvironmental records from the Barstow Formation, Mojave Desert, USA: Geological Society of America Bulletin, v. 132, no. 1–2, p. 113–129.

MacFadden, B.J., Swisher, C.C., III, Opdyke, N.D., and Woodburne, M.O., 1990, Paleomagnetism, geochronology, and possible tectonic rotation of the middle Miocene Barstow Formation, Mojave Desert, southern California: Geological Society of America Bulletin, v. 102, no. 4, p. 478–493.

Miller, D.M., Gans, P.B., Felger, T.J., and Vazquez, J., 2022, Post-Early Miocene silicic volcanism in the northern Mojave Desert, *in* Miller, D.M., ed., Volcanoes in the Mojave: The 2022 Desert Symposium Field Guide and Proceedings: Joshua Tree, California, Desert Symposium, Inc., p. 124–141.

Patterson, W.A., III, Edwards, K.J., and Maguire, D.J., 1987, Microscopic charcoal as a fossil indicator of fire: Quaternary Science Reviews, v. 6, p. 3–23.

R Core Team, 2020, R: A language and environment for statistical computing: Vienna, Austria, R Foundation for Statistical Computing.

Rhodes, A.N., 1998, A method for the preparation and quantification of microscopic charcoal from terrestrial and lacustrine sediment cores: The Holocene, v. 8, no. 1, p. 113–117.

Schmidt, M.W.I., and Noack, A.G., 2000, Black carbon in soils and sediments: Analysis, distribution, implications, and current challenges: Global Biogeochemical Cycles, v. 14, no. 3, p. 777–793.

Schüpbach, S., Kirchgeorg, T., Colombaroli, D., Beffa, G., Radaelli, M., Kehrwald, N.M., and Barbante, C., 2015, Combining charcoal sediment and molecular markers to infer a Holocene fire history in the Maya Lowlands of Petén, Guatemala: Quaternary Science Reviews, v. 115, p. 123–131.

Scott, A.C., 2010, Charcoal recognition, taphonomy and uses in palaeoenvironmental analysis: Palaeogeography, Palaeoclimatology, Palaeoecology, v. 291, p. 11–39.

Vachula, R.S., 2019, A usage-based size classification scheme for sedimentary charcoal: The Holocene, v. 29, no. 3, p. 523–527, doi: 10.1177/0959683618816520.

Whitlock, C., and Millspaugh, S.H., 1996, Testing the assumptions of fire-history studies: An examination of modern charcoal accumulation in Yellowstone National Park, USA: The Holocene, v. 6, no. 1, p. 7–15.

Whitlock, C., and Larsen, C., 2001, Charcoal as a Fire Proxy, *in* Smol, J.P., Birks, H.J.B., Last, W.M., Bradley, R.S., and Alverson, K., eds., Tracking Environmental Change Using Lake Sediments, Volume 3: Terrestrial, Algal, and Siliceous Indicators: Dordrecht, The Netherlands, Kluwer Academic Publishers, p. 75–97.

Wickham, H., François, R., Henry, L., and Müller, K., 2022, dplyr: A grammar of data manipulation, https://dplyr.tidyverse.org.

Woodburne, M.O., Tedford, R.H., and Swisher, C.C., III, 1990, Lithostratigraphy, biostratigraphy, and geochronology of the Barstow Formation, Mojave Desert, southern California: Geological Society of America Bulletin, v. 102, p. 459–477.

Woodburne, M.O., 1996, Precision and resolution in mammalian chronostratigraphy: Principles, practices, examples: Journal of Vertebrate Paleontology, v. 16, no. 3, p. 531–555.

Wynn, J.G., 2007, Carbon isotope fractionation during decomposition of organic matter in soils and paleosols: Implications for paleoecological interpretations of paleosols: Palaeogeography, Palaeoclimatology, Palaeoecology, v. 251, p. 437–448.

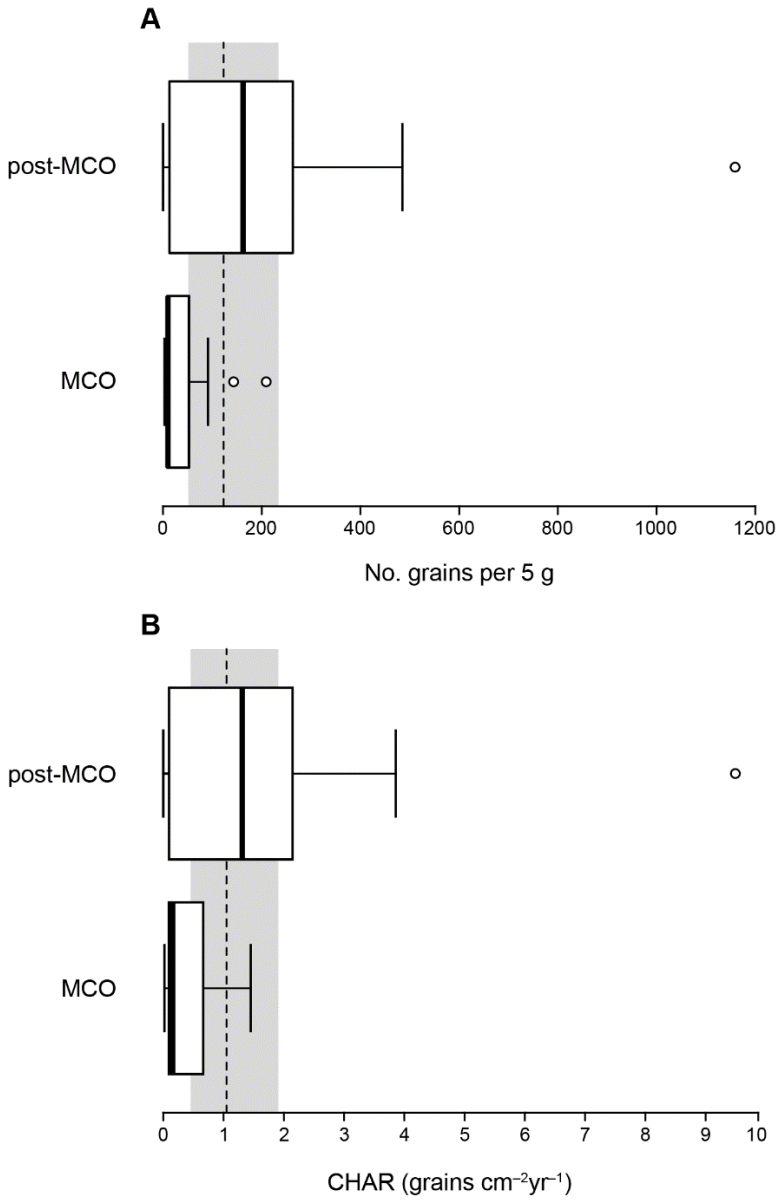

FIGURE S1. (A) Black carbon concentration and (B) Charcoal-accumulation rates (CHAR) from the Barstow Formation, comparing samples deposited during the Miocene Climatic Optimum (MCO) and samples deposited after the MCO. (A) Dashed line shows mean concentration of all samples (122.7), gray shading shows 95% confidence interval (48.9 to 253.7). (B) Dashed line shows mean CHAR of all samples (1.05 grains cm^{-2} yr^{-1}), gray shading shows 95% confidence interval (0.45 to 1.91 grains cm^{-2} yr^{-1}).

TABLE S1. Sediment-accumulation rates (SAR) for facies associations of the Barstow Formation. See Loughney and Badgley (2017).

Facies Association	Dominant lithologies	SAR (m/Myr)	SAR (cm/yr)
6	Siltstone, marl, sandstone	149	0.0149
5	Bentonitic siltstone, claystone	120	0.0120
4	Amalgamated sandstone	357	0.0357
3	Siltstone, marl, sandstone	266	0.0266
2	Thin-bedded claystone, siltstone, marl, sandstone	306	0.0306
1	Sandstone and conglomerate	309	0.0309

TABLE S3. Locations, facies associations (FA), approximate ages, and charcoal-accumulation rates (CHAR) of 26 sediment samples from the Barstow Formation, California. Many of the sample localities are fossil sites, and coordinates are approximated in order to protect the locations. Coordinates are in WGS84.

Sample number	Locality name	Approximate coordinates	FA	Age (Ma)	Counts	CHAR (grains cm^{-2} yr^{-1})
TT-2-6	Truck Top Wash	35.060°, −117.103°	6	13.27	263	2.15
TT-2-2	Truck Top Wash	35.060°, −117.103°	6	13.46	246	1.98
TT-1-15-11	Truck Top Wash	35.061°, −117.103°	6	13.47	485	3.86
TT-1-2	Truck Top Wash	35.061°, −117.103°	6	13.48	1159	9.49
TT-1-15-2	Truck Top Wash	35.061°, −117.103°	6	13.48	40	0.32
TT-1-15-10	Truck Top Wash	35.061°, −117.103°	6	13.48	160	1.29
TT-1-15-9	Truck Top Wash	35.061°, −117.103°	6	13.50	12	0.10
RH-15-1-1	Rodent Hill Basin	35.047°, −117.077°	6	13.77	164	1.34
OC-2-9	Owl Canyon	35.022°, −117.024°	5	13.78	0	0.00
OC-1-7	Owl Canyon	35.039°, −117.025°	5	13.89	13	0.08
FW-3-9	Falkenbach Wash	35.058°, −117.087°	6	14.14	41	0.32
OC-2-8	Owl Canyon	35.022°, −117.024°	5	14.59	8	0.05
FE-16-5	RAM V98004	35.042°, −117.065°	6	14.60	143	1.11
OC-2-7	Owl Canyon	35.022°, −117.024°	5	14.88	3	0.02
FW-2-15-3	Falkenbach Wash	35.058°, −117.085°	5	14.98	209	1.35
OC-2-6	Owl Canyon	35.022°, −117.024°	2	15.13	10	0.16
RB-16-5-2	Valley View Quarry	35.030°, −117.042°	4	15.26	12	0.23
OC-2-3	Owl Canyon	35.022°, −117.024°	2	15.52	10	0.15
CUP-3-2	Camp Quarry	35.027°, −117.048°	3	15.74	9	0.12
COO-2-15-2	Steepside Quarry	35.032°, −117.060°	3	15.90	64	0.96
OC-1-4	Owl Canyon	35.039°, −117.025°	2	15.97	91	1.45
CUP-1-4-2	Cal-Uranium Prospect Canyon	35.025°, −117.048°	3	16.01	10	0.13
CUP-1-4-1	Cal-Uranium Prospect Canyon	35.025°, −117.048°	3	16.04	3	0.04
OC-1-6	Owl Canyon	35.039°, −117.025°	2	16.23	4	0.06
CUP-1-6	Cal-Uranium Prospect Canyon	35.025°, −117.048°	3	16.36	9	0.13
OC-1-3	Owl Canyon	35.039°, −117.025°	1	16.48	23	0.36

TABLE S4. Number of samples, number of counted charred particles, and average charcoal-accumulation rates (CHAR) from sediment samples from the Barstow Formation, California, deposited during and after the Miocene Climatic Optimum (MCO). Difference in median grain count for MCO and post-MCO samples is statistically different from 0 (Wilcoxon Rank Sum test, 95% CI: 2.99–243.00, W=124.5, p=0.02).

	Number of samples	Total number of grains	Average number of grains	Average CHAR (grains cm^{-2} yr^{-1})
Post-MCO	10	2542	254.2 ± 352.2	2.1 ± 2.9
MCO	16	649	40.6 ± 59.6	0.4 ± 0.5

Description of bootstraping and jackknifing procedures in R to generate 95% confidence intervals on charred-particle abundance and charcoal-accumulation rates (CHAR) for the Barstow Formation, California.

Bootstrapping function to generate confidence intervals on charred-particle abundance and CHAR for the entire formation. From strata.uga.edu/8370/lecturenotes/resampling.html.

```
bootstrapMean <- function(x) {
bootstrappedSample <- sample(x, size=length(x), replace=TRUE)
theMean <- mean(bootstrappedSample)
theMean
}
```

Jackknife function to generate confidence intervals on charred-particle abundance and CHAR for each facies association. From strata.uga.edu/8370/lecturenotes/resampling.html.

```
jackknifeMean <- function(x) {
pseudovalues <- vector(length=length(x), mode='numeric')
theMean <- mean(x)
for (i in 1:length(x)) {
jack <- x[-i]
jackMean <- mean(jack)
pseudovalues[i] <- theMean - (length(x)-1)*(jackMean-theMean)
}
estimate <- mean(pseudovalues)
n <- length(pseudovalues)
SE <- sd(pseudovalues)/sqrt(n)
alpha <- 0.05
lowerCL <- estimate + qt(p=alpha/2, df=n-1) * SE
upperCL <- estimate - qt(p=alpha/2, df=n-1) * SE
return(c(lowerCL, upperCL))
}
```

Load charcoal data file.

```
charcoalData <- read.csv("charcoalData.csv", header=TRUE, stringsAsFactors=FALSE)
```

Bootstrap grain counts to generate confidence intervals.

```
set.seed(722)
alpha <- 0.05
bootstrapCounts <- replicate(1000, bootstrapMean(charcoalData$CharCount))
lowerCountLevel <- quantile(bootstrapCounts, alpha/2)
upperCountLevel <- quantile(bootstrapCounts, 1-alpha/2)
```

Bootstrap CHAR values to generate confidence intervals.

```
bootstrapChar <- replicate(1000, bootstrapMean(charcoalData$faCHAR))
lowerCharLevel <- quantile(bootstrapChar, alpha/2)
upperCharLevel <- quantile(bootstrapChar, 1-alpha/2)
```

Subset samples by FA

```
faSixSamples <- dplyr::filter(charcoalData, Facies==6)
faFiveSamples <- dplyr::filter(charcoalData, Facies==5)
faFourSamples <- dplyr::filter(charcoalData, Facies==4)
faThreeSamples <- dplyr::filter(charcoalData, Facies==3)
faTwoSamples <- dplyr::filter(charcoalData, Facies==2)
faOneSamples <- dplyr::filter(charcoalData, Facies==1)
```

Calculate jackknifed confidence intervals on grain counts for each facies association.

```
jackknifeMean(faSixSamples$CharCount)
[1]  27.13089 515.46911

jackknifeMean(faFiveSamples$CharCount)
[1] -66.29109 159.49109

jackknifeMean(faThreeSamples$CharCount)
[1] -12.42416  50.42416

jackknifeMean(faTwoSamples$CharCount)
[1] -37.43895  94.93895
```

Calculate jackknifed confidence intervals on CHAR values for each facies association.

```
jackknifeMean(faSixSamples$faCHAR)
[1] 0.1965198 4.1936568

jackknifeMean(faFiveSamples$faCHAR)
[1] -0.4314625  1.0317512

jackknifeMean(faThreeSamples$faCHAR)
[1] -0.2012464  0.7530760

jackknifeMean(faTwoSamples$faCHAR)
[1] -0.6004883  1.5138067
```